J. Fluid Mech. (1973), *vol.* 61, *part* 4, *pp.* 753–767
Printed in Great Britain

Oscillating flow over a cylinder at large Reynolds number

By H. A. DWYER
Department of Mechanical Engineering, University of California, Davis
AND W. J. McCROSKEY
U.S. Army Air Mobility Research and Development Laboratory, Moffett Field, California

(Received 13 September 1972 and in revised form 27 July 1973)

The boundary-layer flow over a circular cylinder at a Reynolds number of $1{\cdot}06 \times 10^5$ has been studied both experimentally and theoretically. The investigation was designed to concentrate on the self-induced oscillations occurring in the flow; at this Reynolds number, these oscillations have generally been ignored heretofore. In the experimental part of the investigation both the inviscid flow and boundary-layer flow reversals were measured as functions of time. The theoretical part of the study started with the measured inviscid flow and calculated all the boundary-layer characteristics. The boundary-layer calculations themselves revealed some very interesting fine-scale structure of the flow, which strongly indicated that the vanishing of wall shear does not signal the onset of separation for unsteady flow. In general, the agreement between the theoretical calculations and the experimental results was excellent and the unsteady component of this supposedly steady flow was found to be very significant.

1. Introduction

The flow over a circular cylinder has served as a reference problem for many investigations during the development of fluid mechanics over the years and the characteristics of this flow have been well documented over a large range of Reynolds numbers (Achenbach 1968; Morkovin 1964). However, there are regimes of Reynolds number, even for this flow, where our knowledge is very meagre. In the present investigation the self-induced oscillations in the flow over a circular cylinder at $Re = 1{\cdot}06 \times 10^5$ have been studied up to the point of 'separation' (the oscillations are caused by a periodic shedding of vorticity in the wake). The study contains experimental measurements of the details of the flow and theoretical calculations of the boundary-layer structure. The experimental part of the investigation consisted of measuring the time-dependent inviscid flow, stagnation-point motion and the location of zero wall shear stress. For the theoretical part of the study a time-dependent numerical calculation has been carried out. This calculation was performed in a moving co-ordinate system and exhibited some interesting double zeros of the wall shear stress. The agreement between theory and experiment was very good and showed that

the unsteady part of the flow was significant. (The agreement with the mean measurements of Achenbach was also very good.)

The present investigation did not study the flow after the laminar flow reversal point and was restricted mainly to the boundary layer, rather than the unsteady wake flow. It is hoped that this study will provide some information on unsteady incompressible boundary layers which will be useful for unsteady flow over oscillating airfoils, and similar problems with unsteady separation.

2. Experimental arrangements and measurements

A cylinder 4 in. in diameter and 7 ft long was mounted in the 7×10 ft test-section wind tunnel of the U.S. Army Air Mobility Research and Development Laboratory. The free-stream velocity was 50 ft/s and the Reynolds number for the air flow over the cylinder was $Re = 1{\cdot}06 \times 10^5$. At this Reynolds number separation was unsteady and laminar; however, for $Re > 3{\cdot}5 \times 10^5$ turbulent reattachment occurred after a relatively steady laminar separation bubble, and the self-induced oscillations decreased considerably. The experiments were confined to the former Reynolds number, since the harmonic content of the time-dependent measurements was confined to a single harmonic, within 5%, as will be seen from the following results. The instrumentation used to measure the inviscid flow and boundary-layer characteristics consisted of the following: (i) static pressure taps, for mean pressure; (ii) heated-film skin-friction gauges, for measuring the variation of the wall shear (McCroskey & Durbin 1972); (iii) a hot-wire probe mounted on slender needles that protruded 0·050 in. above the cylinder wall, to measure the variation of the inviscid flow velocity just outside the boundary layer; (iv) a pair of hot wires 0·020 in. above the cylinder surface, one in the wake of the other, used to detect flow reversal (this corresponds to a relative boundary-layer location $y/\delta \simeq 0{\cdot}4$); and (v) another hot-wire probe placed $\frac{1}{4}$ in. above the cylinder at 90° away from the geometric stagnation point, to provide a reference in time, or phase throughout the oscillation, for the cylinder-mounted sensors. Figure 1 illustrates the approximate location of all the probes on the cylinder and it can be seen that they are mounted approximately at the mid-span location. Laterally displaced static pressure taps all indicated the same pressure distributions, and in the view of this and the large aspect ratio of the cylinder ($l/d = 21$), the flow was considered to be two-dimensional. The cylinder was mounted so that it could be rotated in 1° increments and data recorded as function of time at each angular position.

Before going on to discuss the theoretical calculations, it is convenient first to present the results of the measurements, since they did serve as very useful input to the analysis. The first measurements that were performed consisted of obtaining a measure of the time-averaged 'separation' line through the use of surface oil flow. The oil flow showed that a mean flow reversal occurred at an angular position of $78 \pm 1°$, and this agrees with other measurements of this type at the same Reynolds number (Achenbach 1968). The oil-flow measurements were carried out all along the span of the cylinder with the same accuracy as mentioned previously.

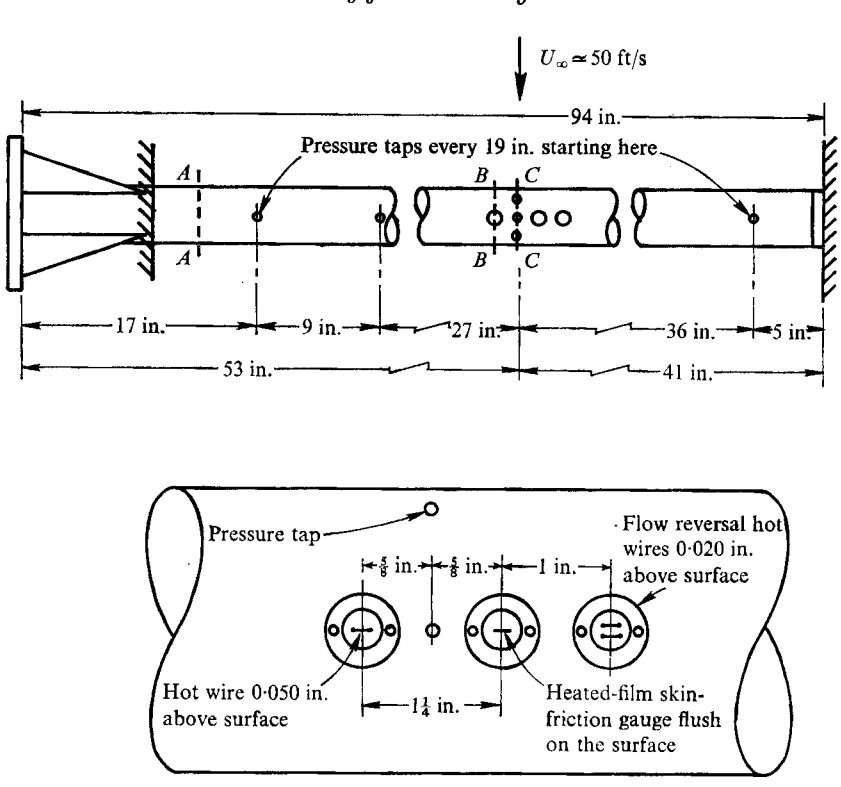

FIGURE 1. Experimental apparatus and instrumentation.

The majority of the measurements are contained in figures 2 and 3. The hot-wire measurements showed the inviscid flow around the cylinder to vary sinusoidally about a mean distribution that agreed well with Achenbach's measurements. At the particular Reynolds number of $1{\cdot}06 \times 10^5$ harmonics higher than the fundamental were indiscernible (less than 5 %) and the phase of the motion was independent of the angular position θ. In other words, the velocity distribution followed a two-term Fourier series

$$U_e/U_\infty = \overline{U}_0 + U_1 \sin(\omega t + \pi) \quad (\omega = 176 \text{ rad/s}),$$

where U_∞ and U_e are the free-stream velocity and local edge velocity, respectively, and $\overline{U}_0$ and U_1 are the local time-average and fluctuating velocities, which are strong functions of θ. Therefore, the values of $\overline{U}_0$ and U_1 were easily determined at each angular position from the maximum and minimum values on the oscillograph traces of U_e. The results, which were the basis of the boundary-layer calculations, are shown in figure 3.

The stagnation-point motion was detected by the dynamic response of the heated-film skin-friction gauges, which exhibited a strong double peak whenever the stagnation point passed over a gauge twice during a cycle. As the cylinder was rotated slowly, the appearance or disappearance of this strong harmonic content marked the limit of the stagnation-point excursion, $\pm 3{\cdot}7°$. This value agrees closely with the amplitude given by the hot-wire fluctuation, see figure 2.

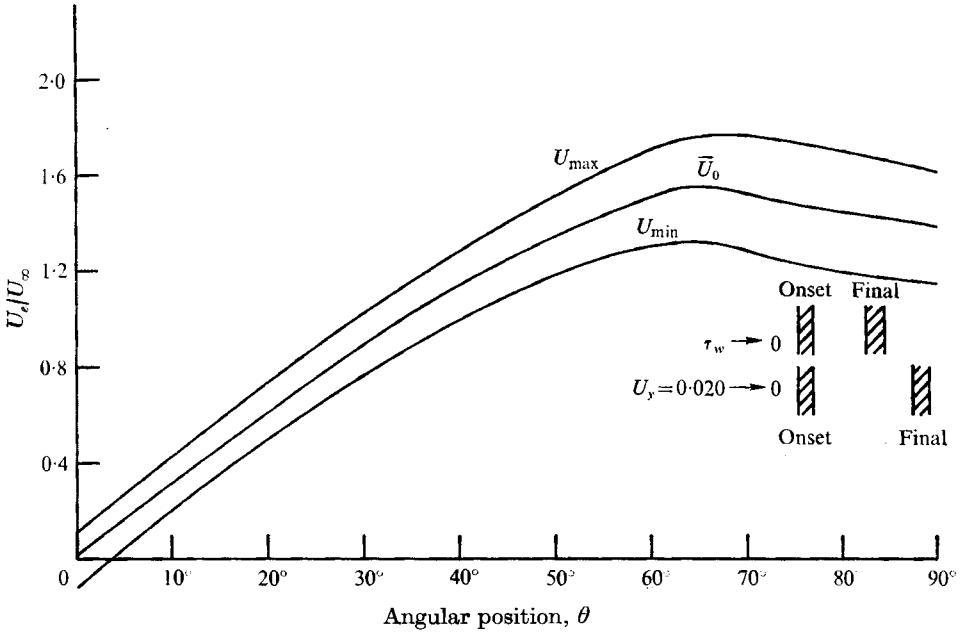

FIGURE 2. Experimental measurements of inviscid flow, flow reversal and zero wall shear stress. $\theta_0 = 3{\cdot}7 \sin \omega t$, $U_e/U_\infty = U_0 + U_1 \sin \omega t$, $U_\infty = 50$ ft/s, $Re = 1{\cdot}06 \times 10^5$, $\omega R/U_\infty = 0{\cdot}59$.

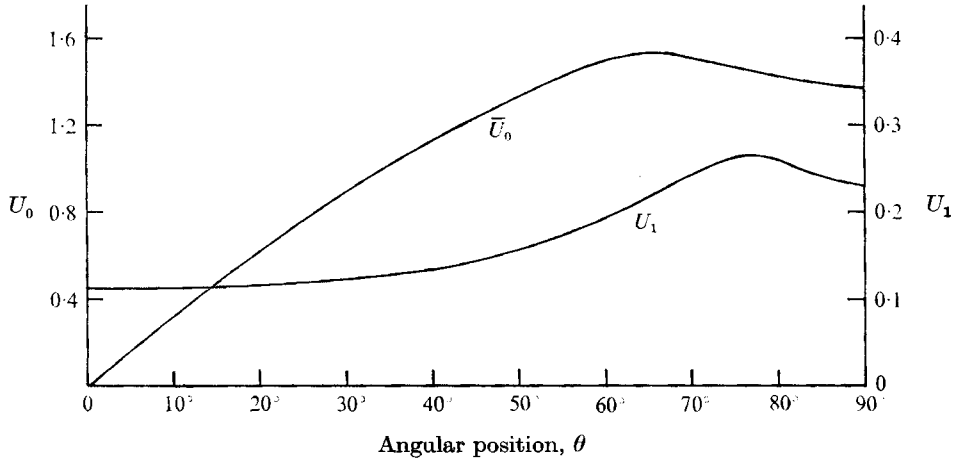

FIGURE 3. Angular distribution of mean and fluctuating components of the inviscid flow.

The stagnation-point motion $\theta_0 = 3{\cdot}7 \sin \omega t$ is sizable and would surely have been given more study in the past if the frequency of the motion were lower. This motion poses a very interesting boundary-layer problem, since a boundary-layer investigation starts at the point of attachment of the fluid particles to the body. The problems that the stagnation-point motion cause in the boundary-layer analysis will be discussed in the next section.

Downstream of the stagnation-point region, the heated-film skin-friction gauge also was used to give the relative variation in the wall shear up to the point of separation, where an abrupt change in the dynamic response of the gauge occurred. Since the separation point moved on the cylinder during each cycle but the gauge remained at a fixed location, two important boundaries could be established by slowly rotating the cylinder. The first was an 'onset' or minimum value of $\theta_s \approx 75°$, where separation first appeared for a brief instant but the flow remained attached during the rest of the cycle. The second was the 'final' or maximum value of $\theta_s \approx 85°$, beyond which the flow was always separated. These results are identified in figure 2 by the symbol $\tau_w \to 0$.

To confirm these measurements further, the double hot-wire probe, mounted slightly above the wall, was used to investigate whether flow reversal had occurred in the vicinity of the zero-shear-stress location. The location of the flow reversal from the double probe is shown in figure 2 by the marks associated with $U_y = 0{\cdot}020 \to 0$. For the minimum value of zero-wall-shear location flow reversal occurred at essentially the same place, thus indicating a sharp breaking away of the boundary layer from the wall. The maximum location of zero wall shear had a flow reversal further downstream, and this may indicate a less sharp breakaway of the boundary layer from the body. Since the flow reversal probe was located at an approximate position $y/\delta = 0{\cdot}4$ in the boundary layer right before flow reversal, this measurement actually indicates that a large portion of the boundary layer had gone through a flow reversal. As will be shown later in the paper, the boundary-layer calculations were carried out only up to this reversal point, except for the very interesting double flow reversal region that occurred in the calculations.

In the present paper no serious attempt will be made to define separation for unsteady boundary layers. The reason why this point was not given more study was that the probes developed only measured wall quantities and that the numerical calculations could only predict the flow in non-reversed regions. Therefore, all the results presented are focused on the position of zero wall shear stress, although it is known that this is not the true separation location. However, both experiments and the calculations indicate that separation is closely related to zero wall shear stress for most of the oscillation cycle. A more detailed discussion of this problem will be given in § 4, and can also be found in the paper by Dwyer & McCroskey (1971), where similar problems were faced for unsteady airfoil flows.

As can be seen from the measurements given above, the mean picture presented by oil flow or other time-averaged techniques misses a large amount of very interesting phenomena for the flow over a cylinder at this Reynolds number. Of course, the present measurements do not give a complete picture of this flow, since they neglect the wake region; however, they do give a detailed picture of the boundary layer. In the next section, a boundary-layer study will be carried out to test our ability to calculate boundary-layer flow in this situation.

3. Boundary-layer analysis

The boundary-layer analysis consisted of two parts: (i) the development of a calculation method for the flow in the vicinity of the moving stagnation points; and (ii) the development of numerical methods for the calculation of the boundary-layer flow in the vicinity of flow reversal. A possibly very difficult third part was eliminated by the use of the measured inviscid flow as a boundary condition for our calculation.

The first major innovation developed was the use of a moving co-ordinate system attached to the stagnation point. Since the stagnation point is accelerating, additional inertial terms must be added to the equations of motion. However, the co-ordinate system is a very natural one, since the flow attaches and develops from the stagnation point, and because the boundary-layer equations take on an interesting form in terms of relative velocities.

Equation 1 is the boundary-layer equation for an accelerating non-rotating moving co-ordinate system. (The terms associated with the rotation of the co-ordinates are small compared with the co-ordinate-system acceleration or are themselves perpendicular to the boundary-layer flow.)

$$\frac{\partial u_R}{\partial t}+u_R\frac{\partial u_R}{\partial x_R}+v\frac{\partial u_R}{\partial y}=-\frac{1}{\rho}\frac{\partial p}{\partial x}+\nu\frac{\partial^2 u_R}{\partial y^2}-a_x, \tag{1}$$

where u_R is the relative velocity, y the boundary-layer co-ordinate, x_R the relative distance from the stagnation point and a_x the stagnation-point acceleration. The pressure-gradient term in the equation represents the actual pressure force on a fluid element; however, if the expression for the pressure gradient from the inviscid flow is used,

$$-\frac{1}{\rho}\frac{\partial p}{\partial x}=\frac{\partial U_e}{\partial t}+U_e\frac{\partial U_e}{\partial x}=a_x+\frac{\partial U_R}{\partial t}+U_R\frac{\partial U_R}{\partial x_R}, \tag{2}$$

then (1) takes the following form:

$$\frac{\partial u_R}{\partial t}+u_R\frac{\partial u_R}{\partial x_R}+v\frac{\partial u_R}{\partial y}=\frac{\partial U_R}{\partial t}+U_R\frac{\partial U_R}{\partial x_R}+\nu\frac{\partial^2 u_R}{\partial y^2}. \tag{3}$$

This equation is interesting since the inertial term resulting from the acceleration of the co-ordinate system does not appear explicitly. It should also be remembered that the expression

$$\partial U_R/\partial t+U_R\partial U_R/\partial x_R$$

does not represent the pressure-gradient force on a fluid element. For the calculations that were carried out in the present paper, (3) was used.

If (3) is employed, the boundary conditions for the problem have to be changed. The outer boundary condition or inviscid flow condition becomes

$$u_R\to U_R=U_e-U_s \quad \text{as} \quad y\to\infty,$$

where U_s is the velocity of the stagnation point. For the wall boundary condition the stationary wall is replaced by a moving one, and the wall condition becomes

$$u_R=-U_s \quad \text{at} \quad y=0.$$

Therefore, in the present problem an observer in the moving co-ordinate system will see the wall oscillating with a sinusoidal motion.

The next problem to discuss is the stagnation-point conditions or the initial conditions for the boundary layer and this problem is best studied in terms of the transformed co-ordinates ξ, η and τ, where

$$\xi = x_R, \quad \eta = y(U_R/2\nu x_R)^{\frac{1}{2}}, \quad \tau = t.$$

In terms of the transformed co-ordinate system, the equations of continuity and momentum become

$$\xi \frac{\partial f'}{\partial \xi} + \frac{\partial f'}{\partial \eta}\frac{\eta}{2}(\beta_x - 1) + \frac{\partial V}{\partial \eta} + \beta_x f' = 0, \tag{4}$$

$$\frac{\xi}{U_R}\frac{\partial f'}{\partial \tau} + \xi f'\frac{\partial f'}{\partial \xi} + \bar{V}\frac{\partial f'}{\partial \eta} = \beta_x(1-f')^2 + \frac{\beta_\tau}{U_R}(1-f') + \frac{1}{2}\frac{\partial f'}{\partial \eta^2}, \tag{5}$$

respectively, where the following definitions have been employed:

$$f' = \frac{u_R}{U_R}, \quad V = v\left(\frac{x_R}{2\nu U_R}\right)^{\frac{1}{2}}, \quad \bar{V} = V + f'\frac{\eta}{2}(\beta_x - 1) + \frac{\beta_\tau}{U_R},$$

$$\beta_x = \frac{\xi}{U_R}\frac{\partial U_R}{\partial x_R}, \quad \beta_\tau = \frac{\xi}{U_R}\frac{\partial U_R}{\partial \tau}.$$

The above transformations and equations do not strictly hold at $x_R = 0$, since $U_R \neq 0$; however, a short distance away from $x_R = 0$ (3–5°) the experimental measurements of the inviscid flow indicated that a useful approximation could be made. In this region the first term on the right side of (5) is significantly larger than the second and $\beta_x \approx 1$. If this is true, then (4) and (5) take on a form similar to that used by Rott (1956) for a stagnation-point flow with an oscillating wall. Therefore, the initial conditions at this point can be approximated by Rotts' solution at a short distance away from $x_R = 0$. Physically, the approximation is equivalent to having the flow dominated by the spatial acceleration away from the moving stagnation point. (Ideally, one would like to have an exact solution like the Rott or stagnation-point solutions starting at $x_R = 0$. However, in the present problem an exact initial condition does not seem to be available unless the full time-dependent Navier–Stokes equations are employed, and this does not seem necessary here.)

The solutions calculated by Rott are not really suitable for use with numerical procedures, since they are not extensive enough for all reduced frequencies $k = \omega/a$ (see Rott's equation). Therefore, exact numerical solutions were obtained for the equations developed by Rott, and these were used in the present investigation. Rott's solutions are suitable for small and large values of k, but can be inaccurate for intermediate ranges. Table 1 gives some tabulated values for the real and imaginary parts of the oscillating solution as a function of η for intermediate values of k. Also given in table 1 are values of the wall derivatives as a function of k (we should like to thank Mr Allan Goldman for his help in obtaining these solutions).

After the determination of a set of initial conditions the numerical solution of (4) and (5) must be tackled. The numerical problem is considerably simplified in

	$k = 1{\cdot}0$		$k = 2{\cdot}0$	
η	g_i	g_r	g_i	g_r
0	0	1·0	0	1·0
0·2	−0·07446	0·8229	−0·12832	0·78848
0·4	−0·11640	0·6566	−0·19424	0·59466
0·6	−0·13350	0·5085	−0·21493	0·42890
0·8	−0·13290	0·3821	−0·20582	0·29529
1·0	−0·12100	0·2785	−0·17969	0·19334
1·2	−0·10310	0·1968	−0·14629	0·11967
1·4	−0·08316	0·1347	−1·11234	0·06932
1·6	−0·06388	0·08927	−0·08191	0·03693
1·8	−0·04692	0·05721	−0·05691	0·01747
2·0	−0·03303	0·03542	−0·03778	0·00670
2·4	−0·01451	0·01219	−0·01458	−0·00085
2·8	−0·00544	0·00361	−0·00473	−0·00135
3·2	−0·00175	0·00091	−0·00129	−0·00068
4·0	−0·00011	0·00003	−0·00005	−0·00006
5·0	0	0	0	0
6·0	0	0	0	0

k	g'_{iw}	g'_{rw}
0·1	−0·049305	−0·81226
0·2	−0·098426	−0·81509
0·5	−0·24292	−0·83429
1·0	−0·46619	−0·89594
2·0	−0·82713	−1·0748
5·0	−0·5001	−1·5974
10·0	−2·1938	−2·2414

TABLE 1. $u = axf'(\eta) + b \exp\{i\omega t\}\, g(\eta)$, $g = g_r + ig_i$, $\eta = y(a/\nu)^{\frac{1}{2}}$

the transformed co-ordinates, since the edge of the boundary layer is usually located at values of η between 3 and 6, and the derivatives of f' with respect to ξ are reduced. This allows the edge of the boundary layer to be determined for practical purposes *a priori* and for relatively large $\Delta\xi$ steps to be taken. The numerical method used to integrate the equations was developed by Dwyer (Dwyer & McCroskey 1971; Dwyer 1972) and consists of an implicit scheme. The equations are evaluated at an unknown grid station and backward differences are taken for the τ and ξ co-ordinates. The η derivatives are evaluated at the unknown station in central-difference form. The resulting set of simultaneous difference equations is solved by use of the Thomas algorithm, since the unknowns appear in a tri-diagonal matrix form (Richtmyer & Morton 1967). This scheme is fast and very stable although the truncation error is only of order $|\Delta t|$ and $|\Delta\xi|$ for the backward differences.

The most interesting feature of the above scheme is that it 'allows' some reversed flow (negative u_R) to be calculated. The scheme will remain stable if the total time-like finite-difference operator

$$1/\Delta t + u_R/\Delta x$$

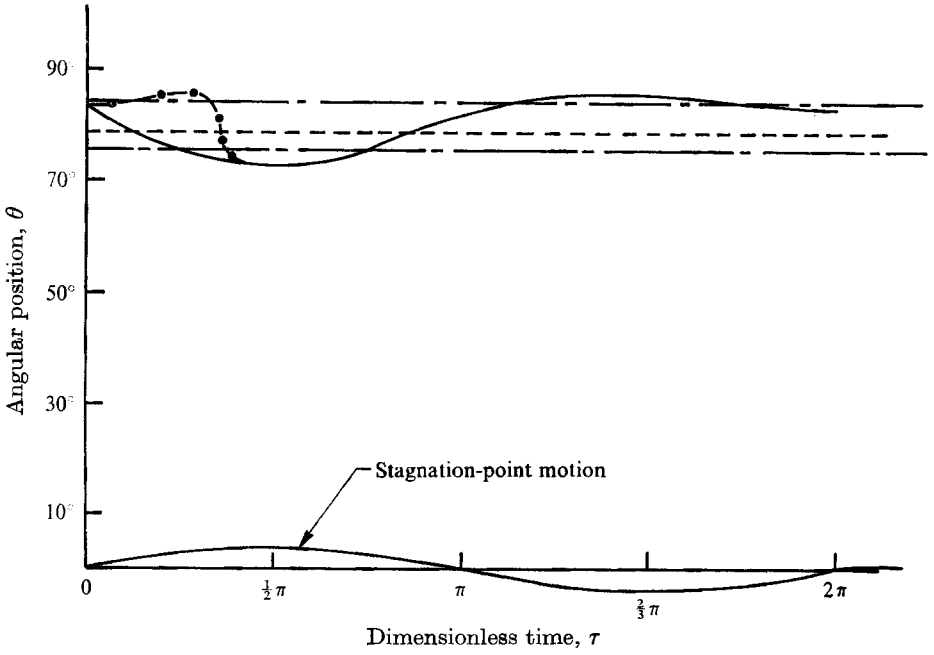

FIGURE 4. Comparison of measured and theoretical zero-shear-stress distributions. – – – –, Achenbach average zero-shear-stress position; ———, time-dependent zero shear stress (calculated); — — —, time-dependent zero-shear-stress limits (measured); — ● —, secondary zero-shear-stress line (calculated).

is positive. In practice this allows for small regions of not too large negative u_R to be calculated. However, since this involves calculating into the history of the flow, the interpretation of these solutions should be cautious. It should be mentioned at this time that the step sizes, Δx and Δt, in the x_R and t directions were always chosen so that convection of vorticity did not proceed downstream at an unphysical rate (that is $\Delta x/\Delta t \leqslant U_R$). In the calculations to be presented in the next section some very interesting regions of reversed flow were found.

4. Results

The numerical calculations were carried out with the inviscid flow measured and the equations developed in the previous sections. For the initial conditions a value of reduced frequency k of 0·32 was found to correspond to the conditions at the stagnation point, and the solution to Rott's equations was used 3° away from $x_R = 0$. Since the Rott solution was not exact, some small oscillations occurred for the first few steps; however, the step size was kept small. After two or three steps of approximately 1°, the numerical solution quickly settled down and remained smooth throughout the calculation. Some of the major results of the calculations are shown in figure 4. In this figure the measured stagnation-point motion, time-dependent zero-shear-stress limits and time-averaged 'separation' point are given along with the calculated time-dependent zero-shear-stress line.

The agreement between the measured limits of zero wall shear stress and the calculated values is very good, the calculations giving slightly larger limits. However, the agreement is within experimental error and it must be concluded that the calculation procedure works quite well. The calculations also show a zero-shear-stress line that oscillates around the measured value of Achenbach's 'separation' point and it must be concluded that 'separation' for this Reynolds number is much more complicated than was previously thought. Another interesting facet of the calculated zero-shear-stress point is that its position is almost 180° out of phase with the stagnation-point motion. If the calculation were quasi-steady it might be expected that the distance between the stagnation point and the zero-shear-stress line may be constant and its motion in phase with the stagnation point. In the present calculations the angular distance between the stagnation point and zero-shear-stress location varies from approximately 70° to 90° and in time is 180° out of phase with the stagnation-point motion. Since the experiments were not designed to measure the time-dependent motion of the zero-shear-stress line, this result has been solely predicted by theory and has not yet been verified experimentally. However, if the measured expressions for the stagnation-point motion and the velocity field are compared,

$$x_s = C_1 \sin \omega t,$$
$$U_e/U_\infty = \overline{U}_0 + U_1 \sin(\omega t + \pi),$$

it is easily seen that they are 180° out of phase.

Figure 4 also contains more very interesting information, and this is associated with the curve labelled 'secondary zero-shear-stress limit'. This curve depicts a boundary-layer phenomenon which seems to be new and is caused by the wall shear stress being first positive then negative, then positive for a short distance, then negative very strongly. The region of the time cycle where this occurs in figure 4 is between 0° and 90° and the phenomenon can be explained clearly with the use of figure 5. In figure 5, and also figures 6 and 7, a normalized skin-friction parameter C_f^*, and also β_x and β_τ^*, is plotted as a function of angular position and time, where

$$\beta_\tau^* = \beta_\tau / U_e.$$

The skin-friction parameter C_f^* is given by the following expression:

$$C_f^* = \frac{\frac{1}{2} C_f Re_x^{\frac{1}{2}}}{(\partial f'/\partial \eta)_S} = \frac{\partial f'/\partial \eta}{(\partial f'/\partial \eta)_S},$$

where

$$C_f = \frac{\mu \, \partial u/\partial y}{\frac{1}{2}\rho u_e^2}$$

and $(\partial f'/\partial \eta)_S$ is the derivative of f' with respect to η at a steady stagnation point. The deviation of C_f^* from one in the vicinity of the stagnation point is a measure of the unsteadiness of the flow (note that all velocities in C_f^* are absolute velocities). The spatial derivatives contained in β_x were calculated numerically from the results in figure 3. The values of β_x can be quite varied, since the magnitude and sign of U_1 vary sinusoidally and β_x depends directly on the time-dependent relative velocity U_R ($= U_e - U_s$). The most interesting variations in β_x occurred near the stagnation point and separation point.

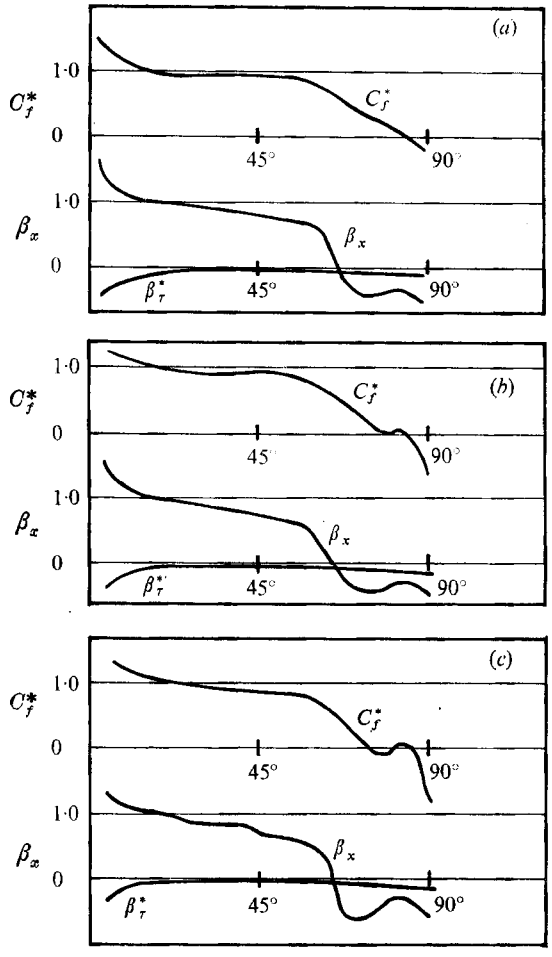

FIGURE 5. Angular distribution of wall-shear-stress and pressure-gradient parameters. (*a*) $\tau = 0$. (*b*) $\tau = \frac{1}{5}\pi$. (*c*) $\tau = \frac{3}{10}\pi$.

Plots for three dimensionless times in a cycle are shown in figure 5 and they correspond to the part of the time cycle between 0° and 90°. At $\tau = 0$ the double flow reversal has not occurred. However, a sign of its coming can be seen by observing the β_x curve, which shows a relative increase after a minimum (from (4) and (5) it can be seen that β_x and β_τ^* are the main parameters which determine the effects of the time-dependent pressure gradient). At $\tau = \frac{1}{5}\pi$, the double zero-shear-stress phenomenon has appeared and is confined to a small region. For the dimensionless time $\tau = \frac{3}{10}\pi$ the region between the double zero-shear-stress locations is significant and occupies almost 15° along the cylinder. The curve for β_x at this time becomes strongly negative around 65° from the geometric stagnation point and then begins to increase. Then β_x reaches a relative maximum before the second zero-shear-stress location and decreases again. From the results of the calculations it can be seen that when β_x increases after a minimum

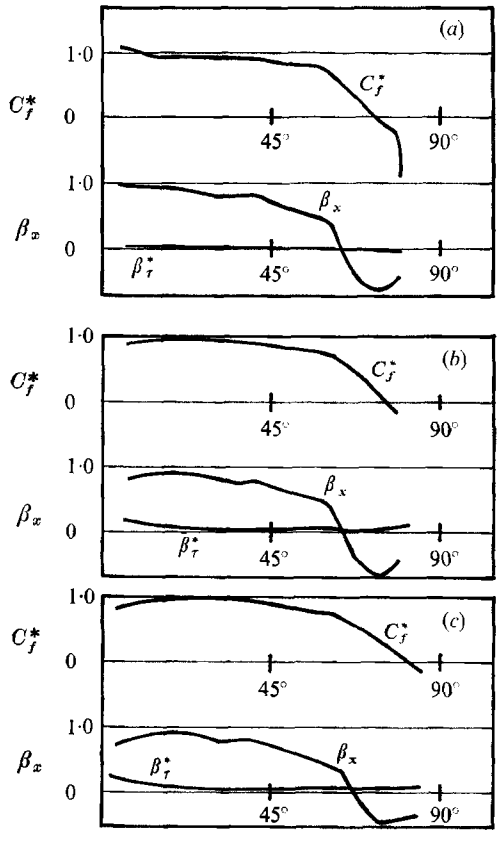

FIGURE 6. Angular distribution of wall-shear-stress and pressure-gradient parameters. (*a*) $\tau = \frac{1}{2}\pi$, (*b*) $\tau = \frac{7}{10}\pi$, (*c*) $\tau = \pi$.

the velocity gradient becomes positive. This is a very interesting phenomenon since β_x is always negative during the reversal, and the values of β_x are large enough that similarity theory would have predicted a strong flow reversal. However, it should be remembered that this boundary layer is time dependent and that the momentum loss due to increased wall shear has not had time to influence the outer regions of the boundary layer. When β_x increases relatively, the outer regions of the flow seem to be capable of transferring enough momentum for the wall shear to again become positive. This phenomenon of the double flow reversal seems to be new, and exhibits a new richness in possible flow fields.

The velocity profiles at various angular locations for $\tau = \frac{3}{10}\pi$ are shown in figures 8(*a*) and (*b*). In figure 8(*a*), it is seen that the velocity profiles begin to become retarded as the first shear reversal is approached, much as in steady flow. At an angular position of 78°, shown in figure 8(*b*), the velocity profile exhibits a region of reversed flow. When the flow reaches 82° the region of reversed flow has disappeared; however, it is obvious from figure 8(*b*) that the boundary layer as a whole has less momentum. At 88° the wall velocities have

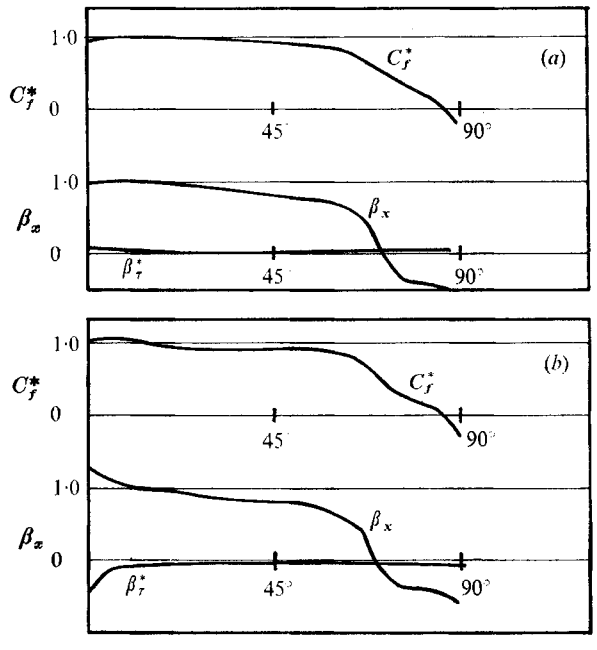

FIGURE 7. Angular distribution of wall-shear-stress and pressure-gradient parameters. (*a*) $\tau = \frac{3}{2}\pi$, (*b*) $\tau = \frac{17}{10}\pi$.

become very large and negative. The adjustment and transfer of momentum in the boundary layer is certainly subtle and rather complex.

The solutions obtained in the first reversed flow region were convergent and the method was very stable. The reason why this behaviour was obtained is directly due to keeping the total time-like finite-difference operator positive,

$$1/\Delta t + u_R/\Delta x \geqslant 0.$$

Also, it can be concluded that the first zero-shear-stress location does not signify separation and that the vanishing of the wall shear is an inadequate description in this time-dependent flow. However, the second zero-shear-stress point seems to have the wall shear decreasing much more rapidly and may be very close to a point of breakaway of the fluid from the body. It should be mentioned that the numerical methods become highly unstable immediately after the second zero-shear-stress location and there does not seem to be any hope of using these methods to proceed further downstream.

Further plots for the skin-friction parameter C_f^* can be found in figures 6 and 7 for the other parts of the time cycle. In general it can be said that these curves have a nature very similar to that for steady flow over a circular cylinder, although the separation point is shifted. At no point in the rest of the cycle does a double zero-shear-stress location occur, and all of the curves indicate that the wall shear becomes strongly negative. For dimensionless times between π and 2π the location of zero wall shear is considerably farther away from the

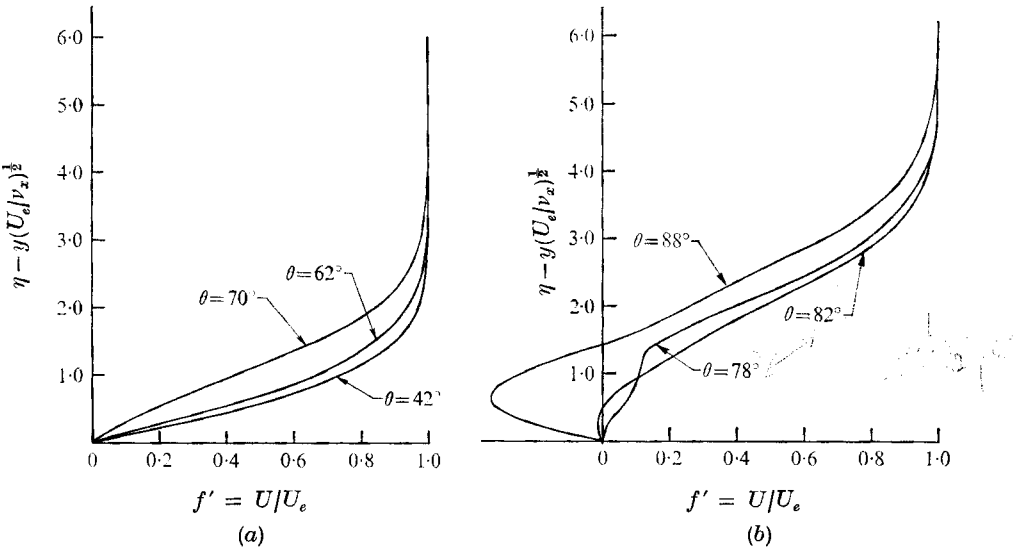

FIGURE 8. Velocity profiles (*a*) before and (*b*) in the flow reversed region.

geometric and actual stagnation points than would be indicated by the mean oil flow studies. The double flow reversal results do not contradict the visual observations of Mattingly (1963), which indicated that a drastic breaking away of the fluid occurs for both the forward and rear location of the flow reversal. As can be seen from figure 4 both the minimum and the maximum points of flow reversal given by the calculations were of the drastic type, and not like the double flow reversal. To obtain an experimental verification of the region of double flow reversal simultaneous measurements of wall shear would have to be carried out with many probes.

A study of all the β_τ^* curves in figures 5–7 indicates that the time-dependent part of the pressure gradient plays a minor role over most of the cylinder except at the stagnation point. A very short distance after the stagnation point the influence of β_x is much greater than that of β_τ^* and the flow is dominated by spatial gradients. For frequencies larger than the ones encountered in the present problem, however, the time-dependent part of the pressure gradient would be more important over a greater spatial distance. In this case new research will be required to handle the flow theoretically.

It should also be mentioned that both positive and negative wall velocities were encountered in the calculation procedure owing to the moving co-ordinate system. The negative velocities might be expected to cause difficulties in the calculation procedure owing to its reversed flow nature. No difficulties were encountered, however, as the time operator was kept positive and also because of the small values of the wall velocity itself.

5. Discussion

The flow over a circular cylinder has again exhibited a very rich collection of flow phenomena, which for the Reynolds number of the present investigation consisted of considerable oscillations in the flow. Although these oscillations are due to an interaction between the wake and the inviscid flow, the use of the boundary-layer approximation is valid before 'separation'. The only region where the boundary-layer approximation may break down is near the stagnation point and even here many of the terms in the full equations will be very small. If a complete numerical simulation of this problem were to be attempted, the main difficulty on the forward portion of the cylinder would be in the determination of the inviscid flow interaction with the wake, and not the interaction between the boundary layer and the inviscid flow.

A part of the investigation that should be viewed cautiously is the calculations which were carried out in the reversed flow region. The use of boundary-layer equations, initial-value equations, to calculate a region of reversed flow is always questionable, since it requires one to march into the history of the problem. However, it seems that some problems are dominated by local pressure gradients and boundary conditions and that inertial and viscous history are not very important. In these circumstances the use of the time-dependent boundary-layer equations to calculate small regions of reversed flow gives good agreement with experimental results. The present problem is an example of this situation.

REFERENCES

ACHENBACH, E. 1968 *J. Fluid Mech.* **34**, 625–639.

DWYER, H. A. 1972 *A.I.A.A. Paper*, no. 72–109.

DWYER, H. A. & MCCROSKEY, W. J. 1971 *A.I.A.A. J.* **9**, 1498–1505.

MCCROSKEY, J. W. & DURBIN, E. J. 1972 *A.S.M.E., J. Basic Eng.* D **94**, 46–52.

MATTINGLY, G. 1963 Private film, Princeton University, New Jersey.

MORKOVIN, M. V. 1964 *A.S.M.E. Symp. Fully Separated Flows, New York*, pp. 102–118.

RICHTMYER, R. D. & MORTON, K. W. 1967 *Difference Methods for Initial Value Problems.* Wiley.

ROTT, N. 1956 *Quart. Appl. Math.* **13**, 444–451.